

Efficient Cloud-Edge Collaborative Inference for Object Re-Identification

Chuanming Wang, Yuxin Yang, Mengshi Qi, Huadong Ma
 Beijing Key Laboratory of Intelligent Telecommunications Software and Multimedia,
 Beijing University of Posts and Telecommunications, China

{wcm, yangyuxin, qms, mhd}@bupt.edu.cn

Abstract

Current object re-identification (ReID) system follows the centralized processing paradigm, i.e., all computations are conducted in the cloud server and edge devices are only used to capture and send images. As the number of videos experiences a rapid escalation, this paradigm has become impractical due to the finite computational resources. In such a scenario, the ReID system should be converted to fit in the cloud-edge collaborative processing paradigm, which is crucial to boost the scalability and practicality of ReID systems. However, current relevant work lacks research on this issue, making it challenging for ReID methods to be adapted effectively. Therefore, we pioneer a cloud-edge collaborative inference framework for ReID systems and particularly propose a distribution-aware correlation modeling network (DaCM) to make the desired image return to the cloud server as soon as possible via learning to model the spatial-temporal correlations among instances. DaCM embeds the spatial-temporal correlations implicitly included in the timestamps into a graph structure, and it can be applied in the cloud to regulate the size of the upload window and on the edge device to adjust the sequence of images, respectively. Traditional ReID methods can be combined with DaCM seamlessly, enabling their application within our proposed edge-cloud collaborative framework. Extensive experiments demonstrate that our method obviously reduces transmission overhead and significantly improves performance. We will release our code and model.

1. Introduction

The object re-identification (ReID) system facilitates users in searching objects accurately across diverse scenes and views, significantly alleviating manual overhead. Serving as a fundamental task in visual surveillance, an increasing number of innovative technologies are being introduced, including elaborate feature extractors [11, 14, 19, 25], data transmission schemes [16], and inference strategies [41], which greatly promote the performance. Consequently, the

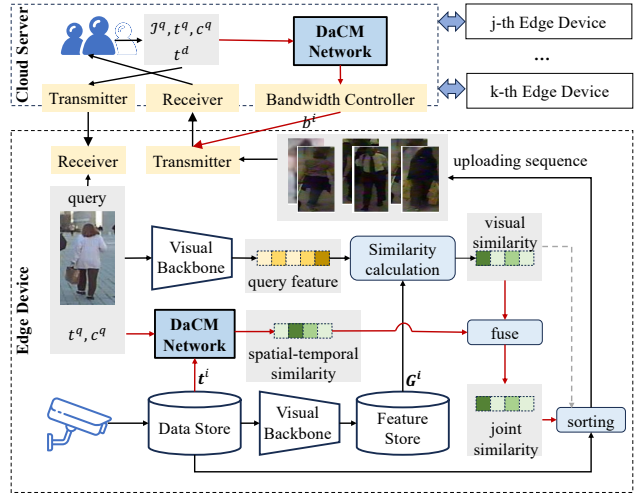


Figure 1. The overview of our approach. The DaCM Network is performed in both cloud server and edge devices for adjusting uploading batch size b^i and image order in the uploading sequence. The red solid denotes the data flow provided by our method, and the gray dashed line denotes the previous data flow without our method.

ReID system has been widely applied to real-world scenarios, playing an important role in traffic monitoring, safety management, etc.

Due to its inherent cross-scene characteristics, the current ReID system mainly comprises one cloud server, multiple edge devices, and a connected network for communication, adhering to centralized processing patterns. The edge devices only capture images and upload them to the cloud server through the connected network, while the cloud server receives them and employs a ReID method for feature extraction and similarity calculation. Ultimately, images are returned to the user in accordance with the resulting similarity. However, with the rapid growth in the number of cameras, such processing patterns put undue pressure on the network bandwidth and computing/storage capacity of the cloud server, which results in considerable service delays and a diminished user experience. Therefore, in line with

the current development trend [2], the ReID system should integrate into a cloud-based collaborative framework.

Previous cloud-edge collaborative visual methods primarily concentrate on the training phase. For instance, FedReID [42] and FedUReID [43] embed the federated learning into ReID system, delving into strategies to exploit distributed data to continuously optimize the feature extractor, thereby enhancing search accuracy. Besides, some works [17] proposes to deploy a segment of the deep neural network to the edge devices, mitigating the computing cost of the cloud server, although it still necessitates a substantial amount of data transmission. We argue that the inference phase holds greater significance for a practical ReID system, and a meticulous scheme should be developed to fully leverage the advantages of both cloud server and edge devices. Therefore, in this paper, in contrast to previous methods, we introduce a pioneering cloud-edge collaborative ReID system, which places a heightened emphasis on optimizing the efficiency of the inference process, a domain that has been underexplored in existing research.

As shown in Fig. 1, in the cloud-edge collaborative framework, one query image is dispatched to each edge device, where it extracts its feature using a local visual backbone and compares this feature with all local gallery images. The resulting similarity sorts the local gallery images to create the uploading sequence. Due to transmission limitations, There is an upper limit to the amount of data a cloud server can accept at one time, so images are uploaded in batches. To achieve an efficient inference, the user’s desired image should be returned to the cloud server promptly. Therefore, two key points in our framework are: (i) the edge device with the desired image should have a higher chance of transmitting the image to the cloud server, and (ii) the desired image should be positioned at the beginning of the upload sequence.

In addition to images, we find that the timestamp is another free launch from the ReID system, which can be effortlessly obtained and utilized to improve the inference. Therefore, to achieve the above goals, we specifically introduce a distribution-aware correlation modeling network (DaCM), transforming learning spatial-temporal correlation into a classification problem. Initially, it embeds spatial-temporal information into a graph structure, followed by several graph convolutional layers to propagate information from to all nodes representing cameras. Finally, we predict the probability that the target will appear on each camera according to the produced node features. Having learned the camera network topology, DaCM can be deployed on the cloud server to allocate transmit chances for each device, and also be deployed on the edge device to re-rank the image sequence. Promisingly, DaCM also enables the system to perform time-constrained ReID (tcReID), i.e. given a target time, the system can return the temporally closest

image of the same identity, which is a more challenging task but not effectively addressed by previous methods.

Furthermore, since we propose a new ReID paradigm (cloud-edge collaborative inference) and task (tcReID), traditional evaluation protocols do not fully showcase its capabilities. Thus, we propose several new evaluation protocols including mean Transmission Number (mTN), Precise Rank@K (pR-K), and mean Precise Rank (mpR). Extensive experimental results demonstrate that our method not only significantly improves traditional evaluation performance but also enhances bandwidth utilization, and reduces searching time, showcasing its superiority. The contributions of our work can be summarised as:

- We propose a cloud-edge collaborative inference framework for ReID system, which can fully use both the advantages of cloud and edges for efficient inference.
- We design a distribution-aware correlation modeling network to model the spatial-temporal correlations, which boosts the efficiency of the system via enlarging the return probability of the desired image.
- We introduce several evaluation protocols and conduct extensive experiments on various benchmark datasets to demonstrate the superiority of our method.

2. Related Work

2.1. Object Re-identification

Object re-identification (ReID) is one of the most important tasks in visual surveillance. It aims at associating person/vehicle images with the same identity captured by different cameras in diverse scenarios. Earlier methods are type-specific, relying on specific attributes of the object, and are applicable only to a particular type of objects, such person ReID [1, 4, 38, 39] and vehicle ReID [22–24]. As methods continue to advance, there is a growing trend towards developing generic ReID methods that are agnostic to the type of object being applied. The focus is on creating general deep learning technologies, including feature extractors [11, 14, 19, 25], metric strategies [36], and loss functions [4, 31]. FastReID [10] integrates the majority of the above techniques, and a simple ResNet50 [9] backbone can deliver outstanding performance on both person ReID and vehicle ReID datasets. He et al. [11] propose a model named TransReID, which adopts the Vision Transformer [7] as the backbone and achieves superior performance for both person and vehicle ReID tasks. All the above methods can be employed in our cloud-edge collaborative framework, partnering with DaCM for efficient inference.

Since spatial-temporal information can be painlessly obtained for ReID data, some ReID methods [5, 13, 33] incorporate it to filter out unreasonable samples. Compared with them, our approach has several obvious differences : (i) Previous methods generate the spatial-temporal distri-

bution through frequency statistics, whereas our approach employs a deep neural network to learn such correlations; (ii) Previous methods still adhere to centralized patterns, whereas our approach is developed within a cloud-edge collaborative framework; (iii) Previous methods only use such information to enhance performance, whereas our approach improves performance while achieving efficient reasoning.

2.2. Cloud-Edge Collaborative Methods

Emerging cloud-edge collaboration approaches showcase their superiority in various systems and communication technologies. Noteworthy instances of these advanced methodologies are evident in seminal works, such as the collaborative occluded face recognition architecture [37], the open-source framework SmartEye for real-time video analytic [34], and the video service enhancement within an edge-cloud collaboration framework [35]. The adaptation of cloud-device collaboration sensitive to changing environments [8], the real-time surveillance video analysis in Cloud-Edge architecture [12], and the Classification Driven Compression framework for reducing deep learning bandwidth consumption [6] further underscore the versatility and impact of these collaborative approaches. Different from these methods, we focus on the ReID task and aim to achieve efficient inference but not model optimization. In particular, we design a cloud-edge collaborative ReID system, in which a DaCM is performed to push the desired image return to the cloud server promptly via modeling the spatial-temporal correlations.

3. Problem Definition

We initially present the problem definition of efficient cloud-edge collaborative inference by outlining the framework’s pipeline and introducing the tasks of ReID.

Given a query image \mathcal{I}^q and its spatial-temporal information $\{l^q, t^q, c^q\}$ (l^q , t^q , and c^q denote the identity ID, taken timestamp, and camera ID, respectively), the ReID system sends these information to every edge device. Then, for the i -th edge device, it extracts the deep feature \mathbf{f}^q from \mathcal{I}^q via the local network and compute the similarity $\mathbf{S} \in \mathbb{R}^{N_i}$ between \mathbf{f}^q and the features $\mathbf{G}^i \in \mathbb{R}^{N_i \times E}$ of all N_i gallery images \mathcal{G}^i , where E is the dimension number of deep features. In conventional methods, the uploading sequence is generated depending solely on \mathbf{S} , but in our approach, we assign the index of each image via considering jointly the visual similarity and spatial-temporal correlations, which can be formulated as:

$$s_j^i = \theta \left(d(\mathbf{f}^q, \mathbf{G}_j^i), e(t^q, c^q, t_j^i, c_j^i) \right), \quad (1)$$

where d denotes the distance function for visual features, e denotes the function of computing spatial-temporal correlations, and θ is used to combine them together.

Then, according to $s^i \in \mathbb{R}^{N_i}$, the uploading image sequence is produced as $\mathcal{U}^i = \{\dots, \mathcal{G}_p^i, \dots, \mathcal{G}_q^i, \dots\}$, which subjects to $0 \leq p, q \leq N_i$, and $s_p^i \leq s_q^i$. As described in the introduction, these images will be uploaded to the cloud server in batches. If the i -th edge device can upload b^i data each time, the transmission number can be formulated as:

$$\text{TN} = \min_i \left(\left\lceil \frac{\epsilon(\mathcal{U}^i)}{b^i} \right\rceil \right). \quad (2)$$

ϵ is an index function that returns the index of the desired image in \mathcal{U}^i , whose implementation is contingent upon user requirements. For example, in the normal ReID task, it is acceptable for the system to just return *one* image with ID l^q , so ϵ represents the index of the first image in \mathcal{U}^i with ID l^q . Note that the procedure is utilized to generate TN , showcasing the efficiency of inference. In a real-world scenario, the gallery image lacks a label, and it needs the user to verify the returned images. Finally, for Eq. (2), we select the minimum transmission number of all edge devices as the final TN. From Eq.(1) and Eq.(2), it is evident that to achieve efficient inference (i.e., minimizing the value of TN), s_j^i of the desired image should be small, and b^i should be large for the edge device containing the desired image. Therefore, the problem can be formulated as reducing TN by learning appropriate s_j^i and b^i from the spatial-temporal information.

In a ReID system, users usually not only seek returned images with the same ID as the query image but also aim to acquire images captured around a specific time, a scenario referred to as time-constrained ReID. So, if the images of one certain target are taken at different times, the sample space of the correct image is narrowed down to a single element. Thus, tcReID is a more challenging variant of ReID, and upon removing the time constraint, tcReID reverts to a normal ReID task.

4. Proposed Approach

In this section, we first describe how the proposed cloud-edge collaborative ReID system works, and how the DaCM network performs within the system to boost its efficiency.

4.1. System Overview

Fig. 1 provides an overview of our proposed cloud-edge collaborative ReID system. The user inputs the request to the cloud server, and the query data is sent to all edge devices along with the bandwidth information b^i produced by the DaCM network in the cloud server. For each device, it employs a receiver to accept the query information and then utilizes a visual backbone to extract deep features of the image. Additionally, the DaCM network takes in the spatial-temporal information of the query image (t^q, c^q) and gallery data (\mathbf{t}^i), and outputs the spatial-temporal correlation, which is fused with the visual similarity to form the

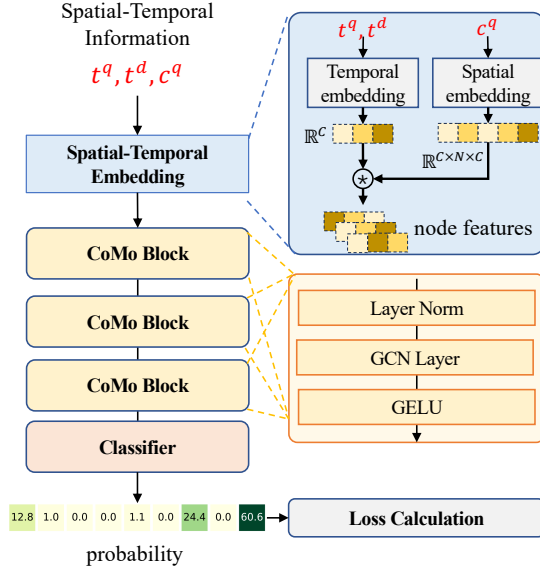


Figure 2. The architecture of DaCM network.

joint similarity. The gallery images are sorted based on the joint similarity to construct the uploading sequence. These images are sent to the cloud server in batches, the size of which is determined by b^i .

4.2. DaCM Architecture

The DaCM network performs an important role in the cloud-edge collaborative ReID system, and in this part we describe its architecture. As shown in Fig. 2, DaCM mainly consists of three components, a spatial-temporal embedding module, multiple Correlation Modeling (CoMo) blocks, and a final classifier.

Spatial-temporal embedding. Inspired by the positional encoding manner used in [32], we adopt the sinusoidal embedding to encode the temporal information. Denoted the query and target times as t^q and t^d , we encode their difference in the formulation of:

$$\begin{aligned} e_{2i} &= \sin\left((t^d - t^q)/\lambda^{2i/D}\right), \\ e_{2i+1} &= \cos\left((t^d - t^q)/\lambda^{2i/D}\right), \end{aligned} \quad (3)$$

where i is the dimension index, $\mathbf{e} \in \mathbb{R}^D$ is the results embedding, and D is the dimension of the embedding. λ denotes the max period of the sinusoidal function. The wavelengths form a geometric progression from 2π to $10000 \cdot 2\pi$.

For the spatial information, considering the fixed localizations of different cameras, we suggest employing learnable parameters $\mathbf{W} \in \mathbb{R}^{C \times D \times C \times D}$ to represent the spatial embedding. C is the number of cameras and the nodes in the graph. When c^q is provided as input, we choose \mathbf{W}_{c^q} as the resulting spatial embedding. This is then combined

with \mathbf{e} to generate a graph structure:

$$\mathbf{A} = \frac{1}{\sum_j^D e_j} \sum_j^D \mathbf{W}_{c^q, j} * e_j + \mathbf{b} \in \mathbb{R}^{C \times D}. \quad (4)$$

Correlation modeling block. As for CoMo blocks, they are used to propagate the information among nodes, and as shown in Fig. 2, one CoMo block is comprised of a Layer Normalization, a GCN layer, and a GELU activation, which can be formulated as:

$$\mathbf{A}^{l+1} = \text{GELU}\left(\mathbf{E}^l \times \text{LN}(\mathbf{A}^l) \times \mathbf{W}^l\right), \quad (5)$$

where $\mathbf{E}^l \in \mathbb{R}^{C \times C}$ is the adjacency matrix, which can be learned during training, and $\mathbf{W}^l \in \mathbb{R}^{C \times C}$ denotes the transfer weight to update the information for each node.

Classifier. Finally, we apply an MLP for each node feature in the graph as the classifier, whose output dimension is set to 1. The outputs of all nodes are concatenated as the final output of the DaCM network:

$$\mathbf{y} = [\text{MLP}(\mathbf{G}_0); \dots; \text{MLP}(\mathbf{G}_{C-1})] \in \mathbb{R}^C. \quad (6)$$

The MLP consists of the sequence of BatchNorm [15], ReLU, and fully connected layers.

4.3. Objective Function

In this part, we describe how to train the DaCM network. For the training set $\mathcal{D}^{\text{train}}$, we randomly select two samples (q and p) with the same label ID but different camera IDs, and their spatial-temporal information is denoted $\{l^q, t^q, c^q\}$ and $\{l^p, t^p, c^p\}$, respectively. According to the time difference $t^p - t^q$ and camera id c^q , we obtain the output \mathbf{y} via the proposed network, and then we optimize the network via the expectation:

$$\arg \max_{\theta} \mathbb{E}_{(q,p) \sim \mathcal{D}^{\text{train}}} [P(y = c^p | t^q, t^p, c^q; \theta)], \quad (7)$$

where θ is the parameters of the network. In implementation, this expectation can be easily converted to a classification problem, and we adopt the cross-entropy loss function to generate the backward gradients:

$$\ell = -\log \frac{\exp(\mathbf{y}_{c^p})}{\sum_i^C \exp(\mathbf{y}_i)}. \quad (8)$$

Actually, the classification solves such a problem: determining the camera at which an object will appear after a duration of $t^p - t^q$, starting from camera c^q . the network will acquire knowledge about the topology of devices deployed in the system and some characteristics of the target's movement, thereby facilitating efficient inference.

4.4. Inference

As discussed in Sec. 3, to achieve efficient inference, the system should promptly return the desired image to the cloud server by generating appropriate e and b . In this section, we elaborate on how to accomplish this goal using the DaCM network.

Cloud-level inference. For cloud-level inference, its emphasis is on assigning a large b^i to the edge devices containing the desired image. Assuming the total bandwidth allocated for C edge devices is B , a simple strategy would be to distribute B equally among edge devices, but it lacks flexibility. We aim to decrease data transmission in the connected network and alleviate stress on the system by dynamically allocating bandwidth to the edge devices based on the spatial-temporal correlation learned in the DaCM network.

Given the query information of $\{\mathcal{I}^q, t^q, c^q, t^d\}$, we send the spatial-temporal information into the DaCM network, and it produces $\mathbf{y} \in \mathbb{R}^C$. The output representation is the chance of the target appearing under each camera at moment t^d . Intuitively, if $\mathbf{y}_i > \mathbf{y}_j$, the i -th edge device should be allocated with a larger bandwidth than the j -th edge device. Thus, we formulate this process as:

$$\hat{b}^i = \text{softmax}(\mathbf{y}/\gamma_0)_i * B, \quad (9)$$

where γ_0 is used to smooth the probability to avoid extreme values. However, it overlooks a crucial factor—the uneven distribution of data among edge devices. The number of images on the edge devices can vary significantly, necessitating the consideration of this factor when allocating bandwidth. Therefore, we finally assign the bandwidth b^i for the i -th edge device as:

$$b^i = \frac{z^i}{\sum_i z^i} * B, \quad z^i = \phi \left(\frac{\mathbf{y}}{\gamma_0} \right)_i * \left(\frac{\exp(|\mathcal{G}^i|)}{\gamma_1 \sum_j \exp(|\mathcal{G}^j|)} \right), \quad (10)$$

where ϕ is the softmax function. Note that for cloud-level inference, t^d should be provided by the user. If there is no such information, and DaCM network does not operate in the cloud.

Edge-level inference. For cloud-level inference, the focus is on re-ranking the index of gallery images in the uploading sequence by generating proper s_j^i as discussed in Eq. (1). Denoted the query image with its spatial-temporal information as $\{\mathcal{I}^q, c^q, t^q\}$, one gallery image at the c^d -th edge device as $\{\mathcal{I}^d, c^d, t^d\}$, we send $\{c^q, t^q, t^d\}$ into DaCM and obtain the output \mathbf{y} . If \mathbf{y}_{c^q} is small, it implies that \mathcal{I}^q and \mathcal{I}^d do not match in spatio-temporal correlation, resulting in a minimal likelihood of having the same ID as the query image. This process can be simply formulated as $\text{softmax}(\mathbf{y})_{c^d}$. Applying this operation to all gallery images on the i -th edge device, we obtain spatial-temporal similarity. Next, we delve into how to combine it with visual similarity.

Given a reliable visual similarity, it is difficult to build a reliable joint metric because the spatial-temporal similarity is unreliable and it is hard to assign appropriate weighting factors for these two types of metrics. Inspired by the joint metric proposed in [33], we adopt a smoothing operator to alleviate unreliable probability estimation. Denoted the spatial-temporal similarity as $\mathbf{o} \in \mathbb{R}^{N_i}$ and the visual similarity as $\mathbf{v} \in \mathbb{R}^{N_i}$, the joint similarity can be computed as:

$$\begin{aligned} s_k^i &= \eta(\hat{\mathbf{o}}_k; \alpha) \eta(\mathbf{v}_k; \alpha), \\ \eta(x; \alpha, \beta) &= \frac{1}{1 + \exp(-\alpha x)}, \\ \hat{\mathbf{x}} &= \text{softmax}(\mathbf{x}/\beta). \end{aligned} \quad (11)$$

Finally, the gallery images are re-ranked according to \mathbf{s}^i .

Time-constrained ReID For a ReID system, users sometimes wish to search for targets near a specific time, a task challenging to accomplish solely based on visual features. Sorting only by time may introduce a large number of unrelated images. Therefore, the key to achieving tcReID lies in how to effectively combine time information with visual information. We observe that Eq. (11) offers a natural way to fulfill such a task. However, Eq. (11) does not satisfy the requirement because it does not introduce t^d into the similarity calculation. Therefore, we propose a new formulation to meet the requirements of tcReID task.

Denoted the query data and target as $\{\mathcal{I}^q, t^q, c^q, t^d\}$, we construct a pattern bank by calculating the correlation between the query image and gallery images in the edge device. DaCM takes in $\{\mathcal{I}^q, t^q, c^q, t^{g_i}\}$ (t^{g_i} is the timestamp of g_i -th gallery image) and output $\mathbf{a}^{g_i} \in \mathbb{R}^C$. This process is applied to all gallery images and we collect them as a pattern bank $\mathbf{B} \in \mathbb{R}^{N_i \times C}$ of \mathcal{I}^q . Then we send the true target time and query data into DaCM and output \mathbf{y} . We calculate the similarity for constructing an uploading image sequence in the form of:

$$\hat{s}_k^i = s_k^i \eta(\cos(\mathbf{B}_k, \mathbf{y})), \quad (12)$$

where \cos denotes the cosine distance function. Finally, we sort the gallery images according to $\hat{\mathbf{s}}^i$ and return them to the cloud server in batches.

5. Experiments

5.1. Experimental Settings

Datasets. We mainly evaluate our proposed framework and method on the DukeMTMC-reID [39] dataset, since it is annotated with high-quality timestamp. It is a subset of DukeMTMC [27] for Person ReID, which has 1,404 identities across multiple cameras, with 408 "distractor" identities. It's split into 702 training and 702 testing IDs. The

training set has 16,522 images, and the testing set includes 2,228 query images and 17,661 gallery images.

Compared methods: We first compare the proposed approach with several inference strategies to show its performance, including:

- *Centralized* denotes the conventional centralized inference strategy, which collects all images captured by edge devices and conducts similarities calculations in the cloud server. We use it as the baseline to show the boosting effectiveness of different inference strategies.
- *Baseline* denotes the simple cloud-edge collaborative inference strategy: the amount of transmission is evenly distributed to each edge device and each edge device assigns the upload sequence according to the distance between the query image and gallery images. By comparing with this strategy, we can see the improvements brought by the proposed DaCM network.
- *stReID* [33] interpolates the statistical spatial-temporal distribution into the similarity calculation process for person ReID. Thus, we can introduce it to the cloud-edge collaborative framework and treat it as one kind of edge-level inference strategies to re-rank the gallery images.
- *Sequence and Pairwise* are two different strategies to compute the spatial-temporal distribution, which are similar to stReID, and we also adopt them as the edge-level inference strategies.
- *Spatula* [16] uses statistical spatial-temporal distributions to prune the video frames for object ReID. Thus, we can adopt it as one kind of cloud-level inference strategies to adjust the amount of transmission of each edge device.
- *Ours(OC)*, *Ours(OE)*, and *Ours* are all our proposed methods. OC and OE denote only cloud-level utilization and only edge-level utilization, respectively. Such comparison can show the effect of these two kinds of utilization applied by the proposed DaCM network.

More details of these strategies can be found in the supplementary materials.

Hyper-parameters: We employ Adam as the optimizer and set its weight decay to $1e-5$. The initial learning rate is set to 0.01 and is reduced by 10 for every 30 epochs. γ_0 and γ_1 are both set to 0.01 as the default. α and β are both set to 0.1. λ in Eq. (3) is set to 10,000 as the default. B is set to $3 * C$, i.e., each edge device can upload an average of three images at a time. More analysis of such hyper-parameters please refer to our supplementary materials.

5.2. Evaluation Protocols

In this part, we first introduce two evaluation protocols (R-K and mAP) that are widely used in previous ReID methods, and then we propose several novel protocols (pR-K, mpR, mTN, and LoA) to show the efficiency and effectiveness of the cloud-edge collaborative inference.

Conventional protocols: For each query, one distance

function is used to compute the similarities between the query image and all the gallery images and return a ranked table from small to large. For each individual query identity, his/her/its gallery samples from the same camera are excluded due to the setting of cross-view matching in ReID. *Rank@K (R-K)* is obtained by checking if top-k gallery images contain the query identity. *Mean average precision (mAP)* is used to evaluate the overall performance. For each query, we calculate the area under the Precision-Recall curve, i.e., average precision (AP). Then, the mean value of APs of all queries, i.e., mAP, is calculated, which considers both precision and recall of a ReID method, thus providing a more comprehensive evaluation.

Proposed protocols: Let us initially provide a definition of the *desired image*, as the proposed protocols hinge upon this conceptual foundation. A desired image is a particular sample among the gallery images, sharing the same identity as the query image and possessing a timestamp in proximity to a given target time.

- *mean Transmission Number(mTN)* is a protocol used to present the efficiency of the method. For each query image, there exists one corresponding TN, and we average the TN of all query images as mTN.
- *precise Rank@K (pR-K)* is calculated by checking whether top-k gallery images contain the desired image that has the same ID with the query image and is closest to the target time, so pR-K is a stricter protocol than R-K.
- *mean precise Rank (mpR)* For the i -th query data, when pR- k_i is successful but pR- (k_i-1) is not successful, we record its precise Rank as k_i , and we average the k_i of all query data as mpR.

In summary, R-K and mAp are used to evaluate the performance of the normal ReID task, mTN is used to evaluate the efficiency of the ReID system, and pR-K and mpR are used to evaluate the performance of the tcReID task. For more details of protocols refer to the supplementary materials.

5.3. Experimental Results

Efficiency of the proposed ReID system. Firstly, we compare the proposed approach with the strategies introduced in Sec. 5.1, and the results are shown in Table 1. By analyzing the mTN values of different strategies, we can see that *Centralized* obtains a huge number of mTN since it requires uploading all images to the cloud server, and a simple cloud-edge collaborative framework (*Baseline*) reduces mTN to 9.56, which saves much network traffic. *stReID*, *Sequence*, and *Pairwise* also yield more promising results than the baseline, but our method achieves the lowest mTN among these methods, demonstrating its efficiency. Meanwhile, the results in the table also show that using DaCM network alone in the cloud server or in the edge devices can reduce the mTN to a certain extent (from 9.56 to 5.39 and

Table 1. Performance of Different Inference Strategies Evaluated on DukeMTMC-reid Dataset. \ denotes the corresponding strategy has no effect on the protocol.

Methods	mAP \uparrow	R-1 \uparrow	R-5 \uparrow	mTN \downarrow	pR-1 \uparrow	mpR \downarrow
Centralized	79.86	90.75	96.77	1561	0.94	123.77
Baseline	79.86	90.75	96.77	9.56	\	\
stReID	82.19	93.67	96.95	4.11	\	\
Spatula	60.17	87.75	92.55	10.01	\	\
Sequence	75.57	90.66	95.87	5.33	\	\
Pairwise	77.06	86.71	93.76	5.45	\	\
Ours(OC)	79.86	90.75	96.77	5.39	\	\
Ours(OE)	89.84	96.68	98.20	4.43	44.74	1.48
Ours	89.84	96.68	98.20	3.25	44.74	1.48
Ours(Lin)	62.43	69.21	73.92	7.05	20.38	20.56
Ours(Sam)	74.16	81.73	86.57	4.76	23.37	9.35

Table 2. Boosting Effect evaluated on DukeMTMC-reID dataset.

Methods	R-1 \uparrow	R-5 \uparrow	R-10 \uparrow	mAP \uparrow
BoW+kissme [38]	25.1	-	-	12.2
LOMO+XQDA [20]	30.8	-	-	17.0
PAN [40]	71.6	-	-	51.5
SVDNet [29]	76.7	-	-	56.8
HA-CNN	80.5	-	-	63.8
APR [21]	70.7	-	-	51.9
Human Parsing [18]	84.4	91.9	93.7	71.0
PSE+ECN [28]	85.2	-	-	79.8
MultiScale [3]	79.2	-	-	60.6
CLIP-ReID [19]	90.0	-	-	80.7
PCB [30]	83.8	91.7	94.4	69.4
PCB + st-ReID [33]	94.0	97.0	97.8	82.8
PCB + InSTD [26]	92.7	96.5	97.6	86.1
PCB + Ours(OE)	96.2	98.3	99.0	89.5
SBS [10]	90.8	95.5	96.8	79.9
SBS + st-ReID	93.7	96.9	97.7	82.2
SBS + Ours(OE)	96.7	98.2	99.0	89.8
TranReID [11]	90.8	95.7	97.3	81.8
TranReID + st-ReID	92.4	96.4	97.5	83.4
TranReID + Ours(OE)	96.8	98.3	98.7	91.0

4.43, respectively), and the combination of them can lead to an optimal result. In addition, we also present the results produced by different spatial-temporal embedding methods (Linear, Sampling, and our used sinusoidal). We can see that the difference in the embedding method can have a huge impact on the results and the sinusoidal embedding used gives the best results.

As for the conventional protocols (mAP/R-1), we can see that stReID boosts the performance from 79.86/90.75

to 82.19/96.95, which is a huge improvement. Our method can further improve the performance of mAP and R-K (89.84/96.58), demonstrating that learning to model the spatial-temporal correlation is better than just simple statistics. As for the protocols of pR-1 and mpR, they are designed to evaluate the performance of the tcReID task, but most of the previous methods do not take it into consideration, and their methods only produce meaningless output. For example, if we use the visual similarity for tcReID, it only achieves 0.94 pR-1. However, we can learn that our method can achieve 44.74 pR-1, which is still low but it demonstrates that the proposed approach can be applied to the challenging task. It is expected that more methods using spatial-temporal correlation will be proposed to solve this problem in the future.

Boosting effect of DaCM for ReID methods. Since the edge-level utilization in our method can be seen as one kind of reranking technologies, we embedded it to several visual ReID methods (PCB [30], SBS [10], TranReID [11]) to show the boosting performance. Methodologies for comparison can be categorized into several different groups, including several classical methods including LOMO+XQDA [20], handcrafted approach BoW+kissme [38], explicit deep learning methods (PAN [40], SVDNet [29] and HA-CNN), attribute-centric techniques APR [21], mask-guided strategies Human Parsing [18], part-based approaches (MultiScale [3] and PSE+ECN [28]), pose-oriented techniques PCB [30], and CLIP-ReID [19]. The results for comparison are shown in Table 2, underscore the noteworthy performance of our approach. Without bells and whistles, our method outperforms all of the existing methods on the DukeMTMC-reID dataset. In addition, the robustness of our methodology is further highlighted when employing the same visual stream method. For instance, integrated with SBS [10], our approach outperforms st-ReID [33], elevating the rank-1 accuracy from 93.7% to 96.7%, and boosting mAP from 82.8% to 89.8%.

5.4. Ablation Study

Selection of different γ_0 and γ_1 . γ_0 and γ_1 are used in Eq. (10) to adjust the bandwidth assigned for each edge devices. Thus, we adjust their different values to show their impact on system performance. The results are shown in Fig. 4. Since these two hyper-parameters only affect the traffic of the connected network, we only present their effect for the protocol of mTN.

Selection of different α and β . α and β are two hyper-parameters used in Eq. 11, which will affect the image order in the uploading sequence. Thus, we conduct two sensitivity analysis experiments to investigate their impact on our ReID system. For the protocol of mTN, we only show the results generated by only using the DaCM network in the

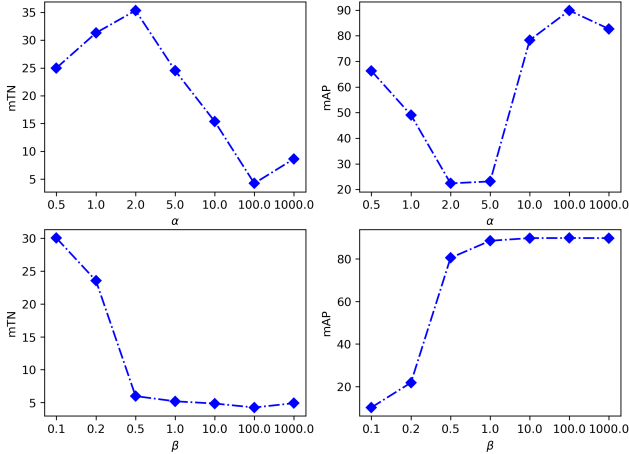


Figure 3. The effects of different values of α (upper) and β (lower) for mTN and mAP.

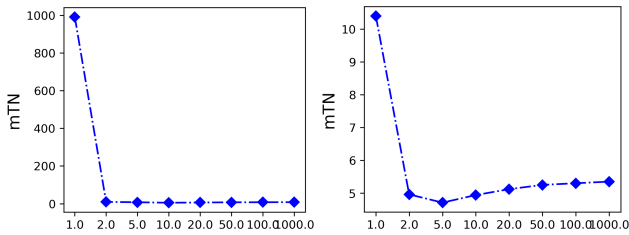


Figure 4. The effects of different values of γ_0 (left) and γ_1 (right) for mTN.

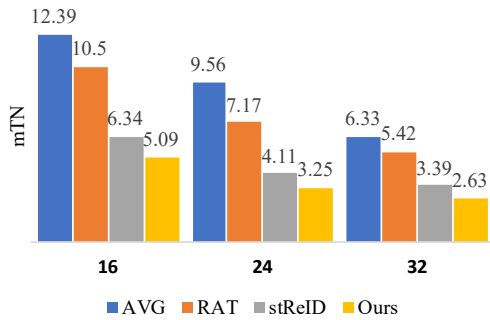


Figure 5. The system performance with different bandwidth limits.

edge devices. As shown in Fig. 3, when α is in the range of 1.0~10.0, the system has much worse performance, and when α is set to 100, the system achieves a low mTN value and a high mAP value. Besides, the performance improves as the value β increases.

Influence of different bandwidth limits B . The bandwidth limits B are important for the ReID system, thus we explore its effect by setting it to 16, 24, 32, respectively, and see the changing of mTN for different strategies. The results are shown in Fig. 5, and we select Average, Ratio, stReID, and ours as the comparison strategies. Their details

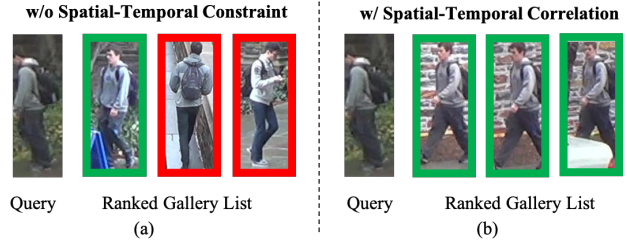


Figure 6. The visualization of retrieval results for some samples from the DukeMTMC-reID dataset. Two sections for baseline and our approach are shown. For each section, the left part represents the query, followed by the ranked retrieval results from the gallery. Persons distinct from the query are highlighted with a red border.

can be referred to the supplementary materials. From the results, we can learn that in all three Settings, our approach achieves the lowest number of data transfers.

5.5. Visualization

To help understand the effect of our approach, we visualized some examples that are corrected by the learned spatial-temporal correlations. The same examples are shown in Fig. 6. The red box indicates inconsistency with the query image ID, while the green box indicates consistency. It is evident that utilizing correlation results in the retrieval of more correct images, leading to the improvement in mAP. More visualized examples please refer to our supplementary materials.

6. Conclusion

In conclusion, the increasing volume of video content makes the traditional centralized ReID system impractical. The current cloud-edge collaborative methods face challenges related to bandwidth constraints and search efficiency. To address these problems, our study introduces a pioneering cloud-edge collaborative ReID framework. Leveraging a distribution-aware correlation modeling network, our approach enables efficient inference, ensuring the desired image returns to the cloud server as early as possible. Comparative experiments with existing ReID methods demonstrate our approach can reduce a huge amount of data transmission, improve performance, and achieve time-constraints ReID, showing its superiority. We also find that the proposed approach requires that the data must have high-quality timestamps, otherwise, the performance will be seriously degraded, which is why we mainly conduct experiments on the DukeMTMC-reid dataset, while other datasets often have various problems with timestamps. Thus, how to use low-quality time information to achieve high-quality correlation learning may be our future research direction.

References

- [1] Ejaz Ahmed, Michael J. Jones, and Tim K. Marks. An improved deep learning architecture for person re-identification. In *CVPR*, pages 3908–3916. IEEE Computer Society, 2015. [2](#)
- [2] Nancy A. Angel, Dakshanamoorthy Ravindran, P. M. Durai Raj Vincent, Kathiravan Srinivasan, and Yuh-Chung Hu. Recent advances in evolving computing paradigms: Cloud, edge, and fog technologies. *Sensors*, 22(1):196, 2022. [2](#)
- [3] Yanbei Chen, Xiatian Zhu, and Shaogang Gong. Person re-identification by deep learning multi-scale representations. In *ICCVW*, pages 2590–2600. IEEE Computer Society, 2017. [7](#)
- [4] De Cheng, Yihong Gong, Sanping Zhou, Jinjun Wang, and Nanning Zheng. Person re-identification by multi-channel parts-based CNN with improved triplet loss function. In *CVPR*, pages 1335–1344. IEEE Computer Society, 2016. [2](#)
- [5] Yeong-Jun Cho, Su-A. Kim, Jae-Han Park, Kyuewang Lee, and Kuk-Jin Yoon. Joint person re-identification and camera network topology inference in multiple cameras. *Comput. Vis. Image Underst.*, 180:34–46, 2019. [2](#)
- [6] Yuanrui Dong, Peng Zhao, Hanqiao Yu, Cong Zhao, and Shusen Yang. CDC: classification driven compression for bandwidth efficient edge-cloud collaborative deep learning. In *IJCAI*, pages 3378–3384. ijcai.org, 2020. [3](#)
- [7] Alexey Dosovitskiy, Lucas Beyer, Alexander Kolesnikov, Dirk Weissenborn, Xiaohua Zhai, Thomas Unterthiner, Mostafa Dehghani, Matthias Minderer, Georg Heigold, Sylvain Gelly, Jakob Uszkoreit, and Neil Houlsby. An image is worth 16x16 words: Transformers for image recognition at scale. In *ICLR*. OpenReview.net, 2021. [2](#)
- [8] Yulu Gan, Mingjie Pan, Rongyu Zhang, Zijian Ling, Lingran Zhao, Jiaming Liu, and Shanghang Zhang. Cloud-device collaborative adaptation to continual changing environments in the real-world. In *CVPR*. IEEE, 2023. [3](#)
- [9] Kaiming He, Xiangyu Zhang, Shaoqing Ren, and Jian Sun. Deep residual learning for image recognition. In *CVPR*, pages 770–778. IEEE Computer Society, 2016. [2](#)
- [10] Lingxiao He, Xingyu Liao, Wu Liu, Xinchun Liu, Peng Cheng, and Tao Mei. Fastreid: A pytorch toolbox for general instance re-identification. In *ACM MM*, pages 9664–9667. ACM, 2023. [2](#), [7](#)
- [11] Shuting He, Hao Luo, Pichao Wang, Fan Wang, Hao Li, and Wei Jiang. Transreid: Transformer-based object re-identification. In *ICCV*, pages 14993–15002. IEEE, 2021. [1](#), [2](#), [7](#)
- [12] Biao Hou and Junxing Zhang. Real-time surveillance video salient object detection using collaborative cloud-edge deep reinforcement learning. In *IJCNN*, pages 1–8. IEEE, 2021. [3](#)
- [13] Wenxin Huang, Ruimin Hu, Chao Liang, Yi Yu, Zheng Wang, Xian Zhong, and Chunjie Zhang. Camera network based person re-identification by leveraging spatial-temporal constraint and multiple cameras relations. In *MMM*, pages 174–186. Springer, 2016. [2](#)
- [14] Su V. Huynh. A strong baseline for vehicle re-identification. In *CVPRW*, pages 4147–4154. Computer Vision Foundation / IEEE, 2021. [1](#), [2](#)
- [15] Sergey Ioffe and Christian Szegedy. Batch normalization: Accelerating deep network training by reducing internal covariate shift. In *ICML*, pages 448–456. JMLR.org, 2015. [4](#)
- [16] Samvit Jain, Xun Zhang, Yuhao Zhou, Ganesh Ananthanarayanan, Junchen Jiang, Yuanchao Shu, Paramvir Bahl, and Joseph Gonzalez. Spatula: Efficient cross-camera video analytics on large camera networks. In *IEEE/ACM SEC*, pages 110–124. IEEE, 2020. [1](#), [6](#)
- [17] Penghao Jiang, Ke Xin, Chunxi Li, and Yinsi Zhou. High-efficiency device-cloud collaborative transformer model. In *CVPR*, pages 2204–2210, 2023. [2](#)
- [18] Mahdi M. Kalayeh, Emrah Basaran, Muhittin Gökmen, Mustafa E. Kamasak, and Mubarak Shah. Human semantic parsing for person re-identification. In *CVPR*, pages 1062–1071. Computer Vision Foundation / IEEE Computer Society, 2018. [7](#)
- [19] Siyuan Li, Li Sun, and Qingli Li. Clip-reid: Exploiting vision-language model for image re-identification without concrete text labels. In *AAAI*, pages 1405–1413. AAAI Press, 2023. [1](#), [2](#), [7](#)
- [20] Shengcai Liao, Yang Hu, Xiangyu Zhu, and Stan Z. Li. Person re-identification by local maximal occurrence representation and metric learning. In *CVPR*, pages 2197–2206. IEEE Computer Society, 2015. [7](#)
- [21] Yutian Lin, Liang Zheng, Zhedong Zheng, Yu Wu, Zhihan Hu, Chenggang Yan, and Yi Yang. Improving person re-identification by attribute and identity learning. *Pattern Recognit.*, 95:151–161, 2019. [7](#)
- [22] Wu Liu, Xinchun Liu, Huadong Ma, and Peng Cheng. Beyond human-level license plate super-resolution with progressive vehicle search and domain priori GAN. In *ACM MM*, pages 1618–1626, 2017. [2](#)
- [23] Xinchun Liu, Wu Liu, Huadong Ma, and Huiyuan Fu. Large-scale vehicle re-identification in urban surveillance videos. In *ICME*, pages 1–6. IEEE Computer Society, 2016.
- [24] Xinchun Liu, Wu Liu, Tao Mei, and Huadong Ma. A deep learning-based approach to progressive vehicle re-identification for urban surveillance. In *ECCV*, pages 869–884, 2016. [2](#)
- [25] Hao Luo, Youzhi Gu, Xingyu Liao, Shenqi Lai, and Wei Jiang. Bag of tricks and a strong baseline for deep person re-identification. In *CVPRW*, pages 1487–1495. Computer Vision Foundation / IEEE, 2019. [1](#), [2](#)
- [26] Min Ren, Lingxiao He, Xingyu Liao, Wu Liu, Yunlong Wang, and Tieniu Tan. Learning instance-level spatial-temporal patterns for person re-identification. In *ICCV*, pages 14910–14919. IEEE, 2021. [7](#)
- [27] Ergys Ristani, Francesco Solera, Roger S. Zou, Rita Cucchiara, and Carlo Tomasi. Performance measures and a data set for multi-target, multi-camera tracking. In *ECCVW*, pages 17–35, 2016. [5](#)
- [28] M. Saquib Sarfraz, Arne Schumann, Andreas Eberle, and Rainer Stiefelhagen. A pose-sensitive embedding for person re-identification with expanded cross neighborhood re-ranking. In *CVPR*, pages 420–429. Computer Vision Foundation / IEEE Computer Society, 2018. [7](#)

- [29] Yifan Sun, Liang Zheng, Weijian Deng, and Shengjin Wang. Svdnet for pedestrian retrieval. In *ICCV*, pages 3820–3828. IEEE Computer Society, 2017. [7](#)
- [30] Yifan Sun, Liang Zheng, Yi Yang, Qi Tian, and Shengjin Wang. Beyond part models: Person retrieval with refined part pooling (and A strong convolutional baseline). In *ECCV*, pages 501–518. Springer, 2018. [7](#)
- [31] Yifan Sun, Changmao Cheng, Yuhang Zhang, Chi Zhang, Liang Zheng, Zhongdao Wang, and Yichen Wei. Circle loss: A unified perspective of pair similarity optimization. In *CVPR*, pages 6397–6406. Computer Vision Foundation / IEEE, 2020. [2](#)
- [32] Ashish Vaswani, Noam Shazeer, Niki Parmar, Jakob Uszkoreit, Llion Jones, Aidan N. Gomez, Lukasz Kaiser, and Illia Polosukhin. Attention is all you need. In *NeurIPS*, pages 5998–6008, 2017. [4](#)
- [33] Guangcong Wang, Jianhuang Lai, Peigen Huang, and Xiaohua Xie. Spatial-temporal person re-identification. In *AAAI*, pages 8933–8940. AAAI Press, 2019. [2](#), [5](#), [6](#), [7](#)
- [34] Xuezhi Wang and Guanyu Gao. Smarteye: An open source framework for real-time video analytics with edge-cloud collaboration. In *ACM MM*, pages 3767–3770. ACM, 2021. [3](#)
- [35] Dapeng Wu, Ruili Bao, Zhidu Li, Honggang Wang, Hong Zhang, and Ruyan Wang. Edge-cloud collaboration enabled video service enhancement: A hybrid human-artificial intelligence scheme. *IEEE TMM*, 23:2208–2221, 2021. [3](#)
- [36] Mang Ye, Jianbing Shen, Gaojie Lin, Tao Xiang, Ling Shao, and Steven C. H. Hoi. Deep learning for person re-identification: A survey and outlook. *IEEE TPAMI*, 44(6): 2872–2893, 2022. [2](#)
- [37] Puning Zhang, Fengyi Huang, Dapeng Wu, Boran Yang, Zhigang Yang, and Lei Tan. Device-edge-cloud collaborative acceleration method towards occluded face recognition in high-traffic areas. *IEEE TMM*, 25:1513–1520, 2023. [3](#)
- [38] Liang Zheng, Liyue Shen, Lu Tian, Shengjin Wang, Jingdong Wang, and Qi Tian. Scalable person re-identification: A benchmark. In *ICCV*, pages 1116–1124. IEEE Computer Society, 2015. [2](#), [7](#)
- [39] Zhedong Zheng, Liang Zheng, and Yi Yang. Unlabeled samples generated by GAN improve the person re-identification baseline in vitro. In *ICCV*, pages 3774–3782. IEEE Computer Society, 2017. [2](#), [5](#)
- [40] Zhedong Zheng, Liang Zheng, and Yi Yang. Pedestrian alignment network for large-scale person re-identification. *IEEE Trans. Circuits Syst. Video Technol.*, 29(10):3037–3045, 2019. [7](#)
- [41] Zhun Zhong, Liang Zheng, Donglin Cao, and Shaozi Li. Re-ranking person re-identification with k-reciprocal encoding. In *CVPR*, pages 1318–1327, 2017. [1](#)
- [42] Weiming Zhuang, Yonggang Wen, Xuesen Zhang, Xin Gan, Daiying Yin, Dongzhan Zhou, Shuai Zhang, and Shuai Yi. Performance optimization for federated person re-identification via benchmark analysis. *CoRR*, abs/2008.11560, 2020. [2](#)
- [43] Weiming Zhuang, Yonggang Wen, and Shuai Zhang. Joint optimization in edge-cloud continuum for federated unsupervised person re-identification. In *ACM MM*, pages 433–441, 2021. [2](#)